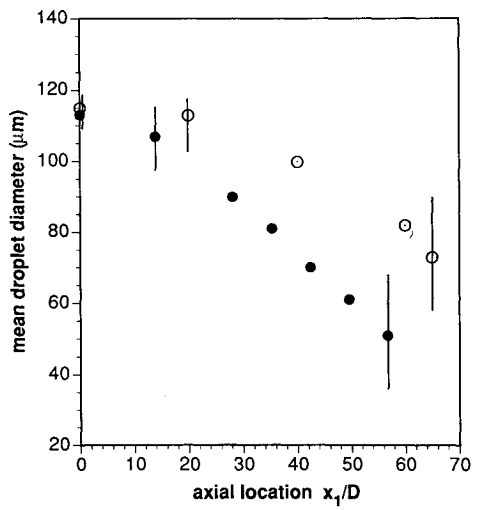

Fig. 3 Pentane droplet diameter as a function of axial distance. Bars represent the scatter in the sampled droplet diameters. •: pentane in heated jet; and o: pentane in unheated jet.

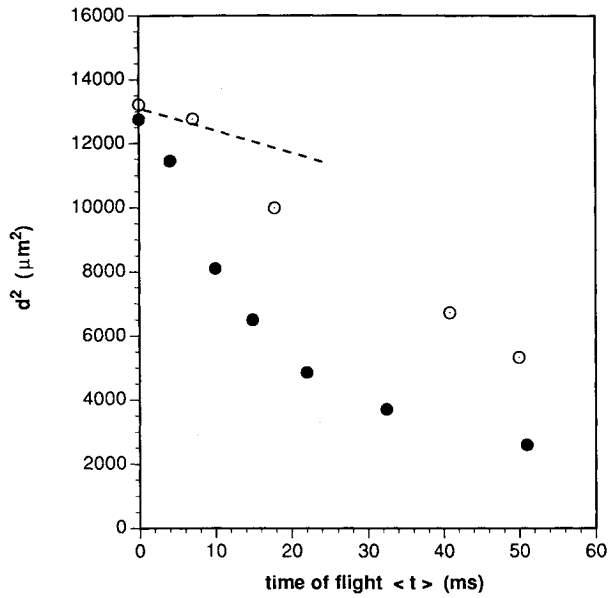

Fig. 4 Pentane droplet diameter squared as a function of mean time of flight from the nozzle exit. Dashed line represents "d^2 law" behavior of a pentane droplet in air at 20° C. •: pentane in heated jet; and o: pentane in unheated jet.

pact of vaporization on droplet drag. This conclusion will be pertinent to combusting sprays in particular.

Figure 3 shows the mean droplet diameter as a function of the axial distance. The droplet diameters were measured with a slide impaction technique. The bars represent the range of diameters which were measured and used to compute the mean diameters. Ten to twenty samples were used for each data point. The diameter data in Fig. 3 are replotted in Fig. 4 using the time-of-flight data. The dashed straight line represents the well-known "d^2 law" for a pentane droplet vaporizing in quiescent air at 20 °C. Because the jet mean temperature is continuously dropping, the pentane droplets in the heated jet experience a declining driving force for vaporization, and thus, do not follow the d^2 law. Call and Kennedy[2] have shown that stochastic simulations[4] do a poor job of reproducing the behavior of the vaporizing droplets. The results suggest that problems may exist with the modeling of droplet vaporization in a turbulent flow.

Acknowledgment

This material is based upon work supported by the U.S. Air Force Office of Scientific Research under Award No. AFOSR-89-0392.

References

[1]Call, C. J., and Kennedy, I. M., "A Technique for Measuring Lagrangian and Eulerian Particle Statistics in a Turbulent Flow," *Experiments in Fluids*, Vol. 12, No. 2, 1991, pp. 125–130.

[2]Call, C. J., and Kennedy, I. M., "Droplet Dispersion, Velocity and Vaporization in Heated and Unheated Jets," AIAA Paper 93–0904, Jan. 1993.

[3]Hinze, J. O., *Turbulence* , McGraw-Hill, New York, 1975, Chap. 6.

[4]Faeth, G. M., "Mixing and Combustion in Sprays," *Progress in Energy and Combustion Science*, Vol. 13, No. 4, 1987, pp. 293–345.

Numerical Simulation of Acoustic Waves in a Combustor Using Total-Variation-Diminishing Schemes

Z. J. Wang,* H. Q. Yang,† and A. J. Przekwas‡
CFD Research Corporation, Huntsville, Alabama 35805

Introduction

COMBUSTION instabilities in liquid and solid rocket engines are organized, large-amplitude unsteady motions of compressible gases coupled with oscillations of the combustion chamber pressure. They occur during steady state as well as during transient operations and result from complex, nonlinear interactions among acoustic waves and heat release processes. One of the major types of combustion instability for liquid-propellant engines is acoustic instability (sound wave amplification). They occur when driving frequencies of propellant atomization, evaporation, and combustion match acoustic resonance frequencies in the chamber components.

Analysis of acoustic amplification by combustion processes in liquid rocket combustion chambers is very difficult due to its very complex nature. In practice, a variety of approximations have been made to simplify the analysis. Many existing analytical models of combustion instability rely on linear stability theory and can generally predict whether an infinitesimal disturbance will grow or decay. There are, however, only a few nonlinear theories of combustion instability, and they are limited by severe assumptions. It is generally recognized that numerical integrations of unsteady Navier-Stokes equations coupled with chemical kinetics and diffusion processes will provide the ultimate solutions. As a first step toward achieving that goal, the Euler equations are employed to simulate the acoustic waves in combustors coupled with variable combustion rate. The state-of-the-art high resolution total-variation-diminishing (TVD) schemes are used to discretize the inviscid flux. These schemes have several favorable properties such as monotonicity preserving, low dissipation, and no problem-specific coefficients. They have achieved great success in modeling compressible flow with strong discontinuities such as shock waves.[1–3] To the authors' knowledge, it has not been fully assessed whether they can resolve the complex flow features in a combustion chamber environment. The current study sets out to address this problem. Four of the most popular TVD limiters are implemented to carry out the simulation. Their dissipation and dispersion errors are assessed by testing on several cases with exact solutions.

Numerical Methodologies

The unsteady Euler equations in integral form can be written as

$$\int_V \frac{\partial}{\partial t}\, dV + \int_s F\, dS = 0 \qquad (1)$$

Presented as Paper 93-0111 at the AIAA 31st Aerospace Sciences Meeting, Reno, NV, Jan. 11–14, 1993; received Feb. 9, 1993; revision received Sept. 21, 1993; accepted for publication Sept. 23, 1993.

*Research Engineer. Member AIAA.
†Group Leader. Member AIAA.
‡VP/Research Projects. Senior Member AIAA.

where Q and F are the vectors of conservative variables and inviscid flux, respectively. Integrating Eq. (1) in a control volume V, we obtain

$$V\frac{\partial}{\partial t}Q + \sum_f F_f \, dS_f = 0 \tag{2}$$

where summation index f represents all surrounding faces of V, Q is the cell average vector of conservative variables, and F_f is the numerical flux function. The determination of numerical flux is fulfilled by a second-order fractional step TVD scheme. This time-stepping procedure can be written as

$$Q^{n+2} = L_i L_j L_k L_k L_j L_i Q^n \tag{3}$$

where L_i, L_j, L_k are second-order operators in i, j, k directions. For example,

$$L_i Q = Q - \frac{\Delta t}{V}(F_{i+1/2} - F_{i-1/2})$$

where Δt is the time step, and

$$F_{i+1/2} = 1/2\,[F_i + F_{i+1} - R_{i+1/2}\,\phi_{i+1/2}] \tag{4}$$

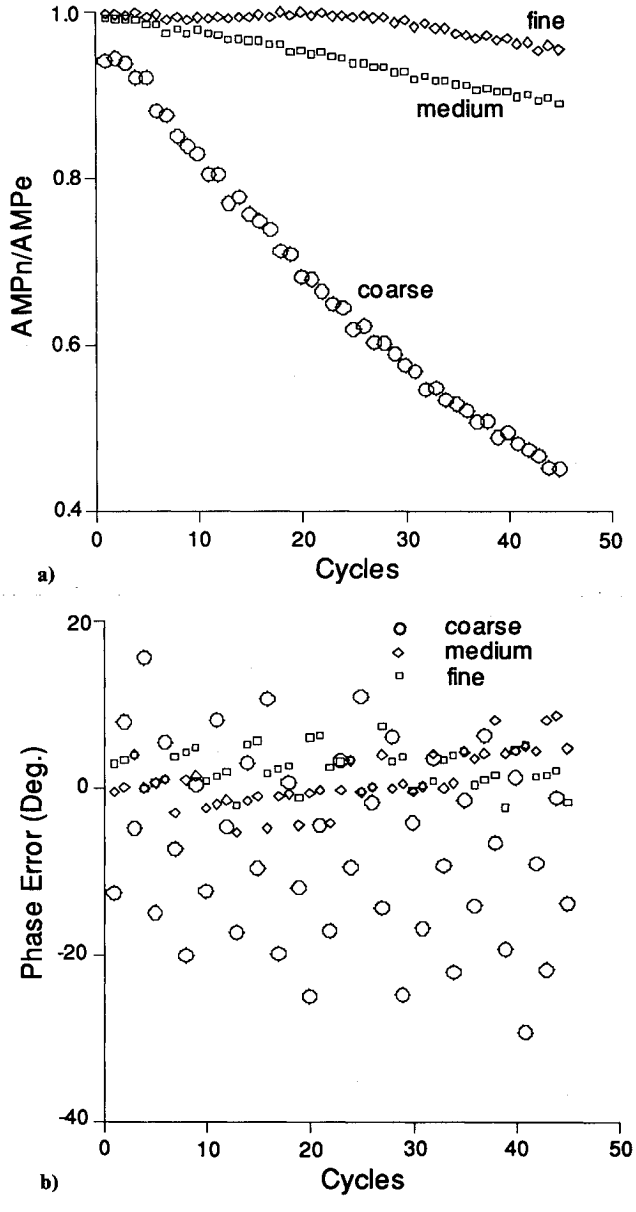

Fig. 1 Damping and phase errors of the numerical solutions with the minmod limiter on three different meshes.

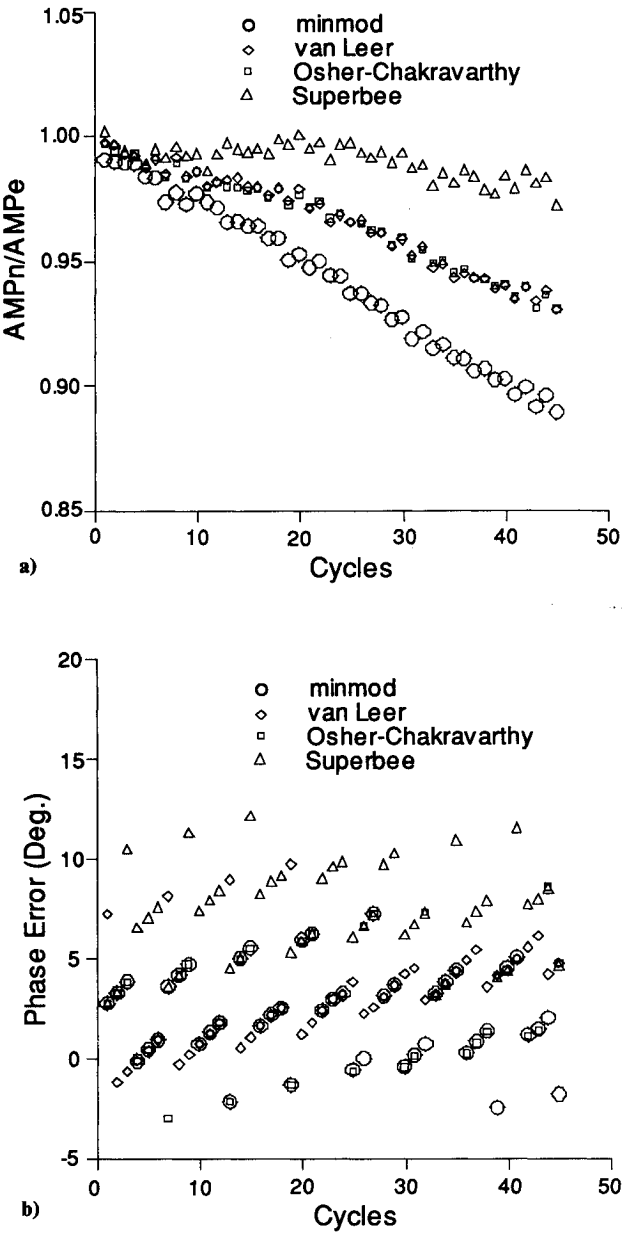

Fig. 2 Damping and phase errors of the numerical solutions with different limiters on the medium mesh.

Here quantities at $i + 1/2$ are calculated by Roe averages.[4] R is composed of right eigenvectors of Jacobian matrix of flux F and each component of ϕ can be written as

$$\phi^l_{i+1/2}\left\{\left|a^l_{i+1/2}\right|\,[1-q\,(r^l_{i+1/2})] + \frac{\Delta t\, dS}{V}\,(a^l_{i+1/2})^2\,q\,(r^l_{i+1/2})\right\}\alpha^l_{i+1/2} \tag{5}$$

with

$$r^l_{i+1/2} = \frac{(\alpha^l_{i+1/2-\sigma})}{\alpha^l_{i+1/2}}, \quad \sigma = \text{sign}\,(a^l_{i+1/2})$$

$$\alpha^l_{i+1/2} = R^{-1}_{i+1/2}\,(Q_{i+1} - Q_i) \tag{6}$$

where a^l ($l = 1,\ldots,5$) are the eigenvalues, and q is a limiter function. Limiters studied here include the most dissipative second-

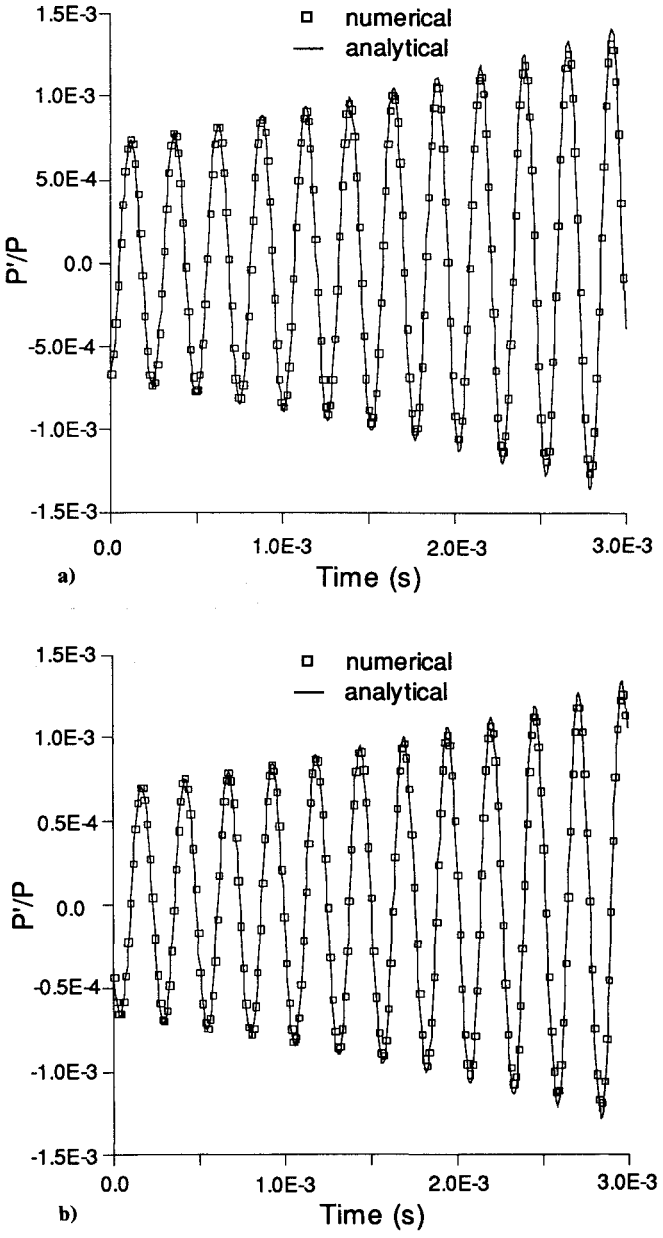

Fig. 3 Comparison of pressure response to a full three-dimensional mode at two different locations: a) at inlet wall, θ = 0 and b) at exit wall, θ = 0.

order limiter—minmod limiter, the most compressive second-order limiter—superbee limiter, a third-order limiter—Osher-Chakravarthy (O-C) limiter and a smooth limiter—van Leer limiter. Mathematically, they can be expressed as the following:

$$q(r) = \text{minmod}(1, r) = \max[0, \min(1, r)] \tag{7}$$

$$q(r) = \max[0, \min(1, 2r), \min(r, 2)] \tag{8}$$

$$q(r) = \frac{1+\phi}{2}\,\text{minmod}(1, \beta r) + \frac{1-\phi}{2}\,\text{minmod}\left(1, \frac{\beta}{r}\right) r \tag{9}$$

with $\phi = 1/3$ and $\beta = 4$.

$$q(r) = \frac{|r| + r}{1 + r} \tag{10}$$

Assessment of TVD Schemes for Acoustics in a Combustor

The combustion instability phenomenon is usually driven by the coupling between heat release from the combustion and the acoustics waves in the combustion chamber. To this end, a simple two-parameter combustion response model proposed by Priem[5] is used. This model relates the burning mass flow rate perturbation $(\rho u)'$ at the injector face to the local pressure disturbance p' and rate of pressure change $\partial p'/\partial t$ in the following form:

$$(\rho u)' = \left(\alpha p' + \beta \frac{\partial p'}{\partial t}\right) \frac{\bar{\rho}\bar{u}}{\bar{p}} \tag{11}$$

where quantities with overbar are mean flow properties and α, β are constants. For the sake of simplicity, the chamber geometry considered is a circular cylinder, and the cylindrical coordinate system (x, r, θ) is employed to describe wave oscillation modes in the chamber. It is further assumed that combustion is completed at the injector face and that gas in the combustion chamber is perfect. Based on these assumptions, Venkateswaran et al.[6] have derived an analytical solution for the linearized problem. In the current simulation, the mean flow conditions are $\bar{p} = 8.6183 \times 10^6$ Pa, $\bar{\rho} = 6.7063$ kg/m^3, $\bar{u} = 352.15$ m/s. The length and diameter of the combustor are 0.3048 and 0.1951 m, respectively.

Two-Dimensional Axisymmetric Modes—Grid Convergence Study

For computational efficiency, we start from the two-dimensional axisymmetric problem with first axial and first radial mode and $\alpha = 1.0$, $\beta = 9.438 \times 10^{-8}$. Three different uniform meshes with 30×20 (coarse), 60×40 (medium), and 120×80 (fine) cells are used to assess the effects of grid resolutions. The minmod limiter is used in this assessment. The exact solutions at $t = 0$ are used as the initial conditions for the numerical simulation. The transient development of the flowfield is then simulated numerically. The initial pressure perturbation is 0.1% to ensure validity of linear assumption.

The ratio between the amplitude of the numerically simulated pressure wave and the exact solution near the centerline of the injector face is plotted in Fig. 1a. The phase error of the numerical solution is plotted in Fig. 1b. It is observed that the numerical solution approaches the exact solution as the computational grid is refined. It is also noticed that the phase error is not a monotonic function of time but rather oscillates around zero. This property is desirable especially for long-term simulations.

Two-Dimensional Axisymmetric Modes—Comparison of Limiters

The performances of different limiters are then assessed using the "medium" 60×40 mesh. The damping and phase errors of different limiters are shown in Fig. 2. Superbee limiter appeared to have the best damping performance, followed by O-C and van Leer limiters. The minmod limiter is the most dissipative. As far as phase errors are concerned, minmod limiter is probably the best, and Superbee limiter is the worst. The best overall performance is achieved by O-C third-order limiter.

Three-Dimensional Modes

To assess the effects of the transverse modes, a full three-dimensional simulation is necessary. Because three-dimensional simulations are much more CPU-intensive than two-dimensional ones, we restrict ourselves to a first tangential and first longitudinal mode. The best performing limiter, O-C third-order limiter is selected in the simulation. A reasonably coarse mesh with $36 \times 36 \times 50$ cells and an H-grid topology in the cross-section is employed. The flow configurations are exactly the same as those in the two-dimensional axisymmetric case. The simulation is carried out until $t = 3$ ms. The pressure oscillations at the injector face and the exit on the chamber wall are plotted against the exact solutions as a function of time in Figs. 3a and 3b. The agreement between the numerical solutions and the exact solutions is quite good considering that the computational mesh is fairly coarse.

Conclusions

Time-accurate, high-resolution TVD schemes have been employed to simulate acoustic waves in an idealized combustion chamber. Available analytical solutions are used to quantify numerical damping and phase errors in these schemes. Generally speaking, high-order TVD schemes have quite small dissipative and dispersive errors. Reasonably good results can be obtained using quite coarse meshes. Particularly, this class of schemes ap-

peared to have bounded dispersive errors. It has been found that the best overall performance is achieved by Osher-Chakravarthy third-order limiter.

Acknowledgments

This work was performed as a part of SBIR Phase II project sponsored by NASA MSFC under a SBIR Phase II contract. The authors are grateful to Paul McConnaughey of NASA MSFC, and to S. Venkateswaran of Penn State University for supplying the analytical solution for the combustion instability problem.

References

[1]Harten, A., "High-Resolution Schemes for Hyperbolic Conservation Laws," *Journal of Computational Physics*, Vol. 49, No. 2, 1983, pp. 357–393.

[2]Chakravarthy, S. R., and Osher, S., "A New Class of High-Accuracy TVD Schemes and Their Applications," *Journal of Computational Physics*, Vol. 68, No. 1, 1987, pp. 151–179.

[3]Yee, H. C., "A Class of High-Resolution Explicit and Implicit Shock-Capturing Methods," NASA TM-101088, Feb. 1989.

[4]Roe, P. L., "Approximate Riemann Solvers, Parameter Vectors and Difference Schemes," *Journal of Computational Physics*, Vol. 43, No. 2, 1981, pp. 357–372.

[5]Priem, R. J., "Round Robin Calculation of Wave Characteristics in a Fixed Geometry-Operating Conditions Liquid Rocket Using Given Simplified Combustion Equations," JANNAF Workshop on Numerical Methods in Combustion Instability, Orlando, FL, Feb. 1990.

[6]Venkateswaran, S., Grenda, J., and Merkle, C. L., "Computational Fluid Dynamic Analysis of Liquid Rocket Combustion Instability," *Proceedings of the AIAA 10th Computational Fluid Dynamics Conference* (Honolulu, HI), AIAA, Washington, DC, 1991, pp. 926–936.

Effect of Imposed Pressure Gradients on the Viscous Stability of Longitudinal Vortices

Robert E. Spall*
University of South Alabama, Mobile, Alabama 36688

I. Introduction

VISCOUS stability calculations of the "q-vortex" [derived from the far-wake solution for a trailing line vortex (Batchelor[1])] have been performed by Lessen and Paillet,[2] Stewartson,[3] and Khorrami.[4] Several other researchers have investigated the inviscid stability of these profiles (Lessen et al.,[5] Duck and Foster,[6] Leibovich and Stewartson,[7] Stewartson and Capell,[8] Duck[9]). Results show that the stability of the vortex is strongly dependent on the value of q (related to the ratio of the maximum swirl velocity to the maximum axial velocity). For instance, the vortex is completely stabilized to inviscid disturbances for values of $q > 1.5$, with the most unstable wave obtained in the limit $|n| \to \infty$ (where n is the azimuthal wave number).

In the present work, the effects of pressure gradients on the viscous stability of longitudinal vortices are investigated. Mean flow profiles computed as numerical solutions to the quasicylindrical equations of motion are employed. This procedure allows one to impose pressure gradients through the boundary conditions at the radial edge of the domain. To this author's knowledge, the effect of imposed pressure gradients on the stability of longitudinal vortices has not yet been studied.

The stability calculations are performed using a normal mode analysis. Although, strictly speaking, a nonparallel stability theory is appropriate [multiple scales (Saric and Nayfeh[10]) or parabolized stability equation approach (Bertolotti[11])], the quasiparallel flow assumption is made. The quasiparallel assumption is justified on the grounds that the spatial development of the vortex is relatively slow; that is, at high Reynolds numbers and under the influence of weak pressure gradients, significant changes occur over many wavelengths. Provisions are made to include some nonparallel effects by retaining radial velocity and streamwise derivative terms in the mean flow. The stability formulation is based on second-order-accurate finite difference approximations on a staggered grid, with the accuracy of the computed eigenvalues being improved through Richardson extrapolation.

II. Problem Formulation

Mean Flow

The linear stability of solutions to the quasicylindrical equations of motion is considered. The quasicylindrical equations are derived from the laminar, incompressible, axisymmetric equations of motion as a result of boundary-layer-type assumptions (Hall[12]) and are given as

$$\frac{\partial u}{\partial r} + \frac{u}{r} + \frac{\partial w}{\partial z} = 0 \tag{1}$$

$$\frac{v^2}{r} = \frac{\partial p}{\partial r} \tag{2}$$

$$u\frac{\partial v}{\partial r} + \frac{uv}{r} + w\frac{\partial v}{\partial z} = \frac{1}{Re}\left(\frac{\partial^2 v}{\partial r^2} + \frac{1}{r}\frac{\partial v}{\partial r} - \frac{v}{r^2}\right) \tag{3}$$

$$u\frac{\partial w}{\partial r} + w\frac{\partial w}{\partial z} = -\frac{\partial p}{\partial z} + \frac{1}{Re}\left(\frac{\partial^2 w}{\partial r^2} + \frac{1}{r}\frac{\partial w}{\partial r}\right) \tag{4}$$

where r and z are cylindrical-polar coordinates; u, v, and w are the radial, swirl, and axial velocity components; p is the pressure, and Re is the Reynolds number. Lengths have been made nondimensional with respect to a length scale l [defined following Eq. (11)], velocities with respect to a velocity scale W_∞, and pressure with respect to ρW_∞^2.

The preceding equations are solved subject to the following boundary conditions:

$$\text{at } r = 0: \quad u = v = \frac{\partial w}{\partial r} = 0 \tag{5}$$

$$\text{at } r = r_0: \quad v = V(z); \qquad w = W(z); \qquad p = P(z) \tag{6}$$

In addition, initial conditions are specified at $z = 0$ as

$$v = v_0(r) \tag{7}$$

$$w = w_0(r) \tag{8}$$

which are derived from Eqs. (10) and (11) later.

In general, the specification of the outer boundary conditions and the radius of the outer boundary may be arbitrarily specified. An exception occurs if the outer boundary represents an inviscid stream surface. In that case, the relationship

$$\frac{u}{w} = \frac{dr}{dz} \tag{9}$$

is implied and only one of r_0, W, or P may be arbitrarily specified. An iterative solution procedure is then implemented such that r_0 takes on a value appropriate for the stream surface defined by Eq. (9). This is the procedure followed in this paper for the pressure gradient cases. That is, the pressure is specified along the outer boundary, which is defined as an inviscid stream surface. The problem is parabolic in the streamwise direction and thus the equations may be solved by marching in z. The quasicylindrical equations were first solved by Hall[13]

Received March 9, 1993; revision received July 26, 1993; accepted for publication Aug. 17, 1993.

*Assistant Professor, Mechanical Engineering.